

RESEARCH ARTICLE

10.1002/2016JA023344

Special Section:

Geospace system responses to the St. Patrick's Day storms in 2013 and 2015

Key Points:

- GICs measured around the world during the 17 March 2015 storm are examined
- Enhanced GIC activity near the equator is observed both at the start and during the storm in different longitude sectors
- Solar wind data indicate that sudden changes in the solar wind dynamic pressure caused the enhanced equatorial GICs

Correspondence to:

B. A. Carter,
brett.carter@rmit.edu.au

Citation:

Carter, B. A., E. Yizengaw, R. Pradipta, J. M. Weygand, M. Piersanti, A. Pulkkinen, M. B. Moldwin, R. Norman, and K. Zhang (2016), Geomagnetically induced currents around the world during the 17 March 2015 storm, *J. Geophys. Res. Space Physics*, 121, 10,496–10,507, doi:10.1002/2016JA023344.

Received 15 AUG 2016

Accepted 9 OCT 2016

Accepted article online 12 OCT 2016

Published online 25 OCT 2016

Geomagnetically induced currents around the world during the 17 March 2015 storm

B. A. Carter^{1,2}, E. Yizengaw², R. Pradipta², J. M. Weygand³, M. Piersanti⁴, A. Pulkkinen⁵, M. B. Moldwin⁶, R. Norman¹, and K. Zhang^{1,7}

¹SPACE Research Centre, RMIT University, Melbourne, Victoria, Australia, ²Institute for Scientific Research, Boston College, Boston, Massachusetts, USA, ³Institute of Geophysics and Planetary Physics, University of California, Los Angeles, California, USA, ⁴Dipartimento di Scienze, Fische e Chimiche, Università di L'Aquila, L'Aquila, Italy, ⁵NASA Goddard Space Flight Center, Greenbelt, Maryland, USA, ⁶Department of Climate, Space Sciences, and Engineering, University of Michigan, Ann Arbor, Michigan, USA, ⁷School of Environment and Spatial Informatics, China University of Mining and Technology, Xuzhou, China

Abstract Geomagnetically induced currents (GICs) represent a significant space weather issue for power grid and pipeline infrastructure, particularly during severe geomagnetic storms. In this study, magnetometer data collected from around the world are analyzed to investigate the GICs caused by the 2015 St. Patrick's Day storm. While significant GIC activity in the high-latitude regions due to storm time substorm activity is shown for this event, enhanced GIC activity was also measured at two equatorial stations in the American and Southeast Asian sectors. This equatorial GIC activity is closely examined, and it is shown that it is present both during the arrival of the interplanetary shock at the storm sudden commencement (SSC) in Southeast Asia and during the main phase of the storm ~10 h later in South America. The SSC caused magnetic field variations at the equator in Southeast Asia that were twice the magnitude of those observed only a few degrees to the north, strongly indicating that the equatorial electrojet (EEJ) played a significant role. The large equatorial magnetic field variations measured in South America are also examined, and the coincident solar wind data are used to investigate the causes of the sudden changes in the EEJ ~10 h into the storm. From this analysis it is concluded that sudden magnetopause current increases due to increases in the solar wind dynamic pressure, and the sudden changes in the resultant magnetospheric and ionospheric current systems, are the primary drivers of equatorial GICs.

1. Introduction

The 17 March 2015 geomagnetic storm has been the largest in more than 10 years (minimum *SYM-H* of -234 nT), and some key aspects of this storm have attracted significant research attention. For example, the resulting ionospheric storm phases have been thoroughly examined [e.g., *Astafyeva et al.*, 2015; *Fagundes et al.*, 2016; *Zhong et al.*, 2016], and the response of the equatorial ionosphere to prompt-penetration electric fields and disturbance dynamos has been investigated [e.g., *Ramsingh et al.*, 2015; *Tulasi Ram et al.*, 2016; *Carter et al.*, 2016; *Huang et al.*, 2016; *Joshi et al.*, 2016; *Zhou et al.*, 2016; *Kakad et al.*, 2016; *Huang et al.*, 2016].

Geomagnetically induced currents (GICs) represent a significant challenge for society, given our strong dependence on stable electricity supply [e.g., *Knipp*, 2015; *Gaunt*, 2016, and references therein]. GICs arise from induced geoelectric fields that are caused by magnetic field fluctuations in the near-Earth space environment via Faraday's law [e.g., *Viljanen*, 1998; *Pirjola*, 2000]. GICs are well known to occur during severe geomagnetic storms, particularly those caused by coronal mass ejections from the Sun.

Reports tasked with providing economic impacts of severe space weather events have generally been focused on one particular country/region (e.g., NAOS report (U.S. National Academy of Sciences, Severe Space weather Events Understanding Societal and Economic Impacts, a workshop report, Washington, DC: The National Academies Press, 2008) and Lloyd's report (Lloyd's: Solar Storm risk to the North American grid, available at: www.lloyds.com, 2013.)). Although, a recent analysis using a global economics model has shown that a 10% reduction in electricity supply to Earth's most populated and highly industrialized regions due to a severe geomagnetic storm can impact the global economy on the same scale as wars and global financial crises [*Schulte in den Bäumen et al.*, 2014].

These serious consequences are based on lengthy power supply loss due to the failure of expensive transformers that take a long time to replace (NAOS report). However, some recent results have shown that catastrophic failures are not necessarily required in order to have a detectable economic impact because of the way that wholesale electricity markets operate. *Forbes and St. Cyr* [2008] studied the impact of space weather on 12 geographically disparate locations around the world and demonstrated that real-time market conditions were statistically related to local magnetic field fluctuations. In another study, *Schrijver et al.* [2014] found that insurance claim rates for industrial electrical equipment across North America rose significantly on days with elevated geomagnetic activity. Therefore, even if power infrastructure hardware is not lost during severe space weather events, GICs in regional power grids can still have broad flow-on effects throughout the global economy, which highlights the continuing need for better understanding of the space environment and its effects on our infrastructure.

Previous research attention has been focused on quantifying and modeling the effects of GICs in the high-latitude region, which is appropriate given that GICs are known to be the most intense in the auroral regions, beneath the auroral electrojets [e.g., *Pulkkinen et al.*, 2005, and references therein]. Some recent studies have shown that the equatorial boundary of the high GIC threat region lies between 50° and 60° magnetic latitude [*Pulkkinen et al.*, 2012; *Ngwira et al.*, 2013; *Love et al.*, 2016].

The middle- and low-latitude regions have also received some research attention [e.g., *Kappenman*, 2003, 2005; *Trivedi et al.*, 2007; *Watari et al.*, 2009; *Marshall et al.*, 2011, 2012; *Zhang et al.*, 2015, 2016] due to the magnetic field variations that are observed during sudden impulses (SIs), which are caused by sudden changes in the solar wind dynamic pressure [e.g., *Russell et al.*, 1994]. When the solar wind dynamic pressure suddenly increases, the magnetopause current suddenly changes, and this results in a global magnetic field signature [e.g., *Araki*, 1977, 1994; *Russell et al.*, 1994; *Shinbori et al.*, 2009]. The magnitude of the resulting magnetic field fluctuation varies significantly with location on the ground, with generally more pronounced effects between 60° and 70° magnetic latitude [*Fiori et al.*, 2014] due to the location of the auroral ionospheric currents at the moment of the SI.

The global magnetic field signature caused by SIs has been the subject of a lot of research. A model for SIs (also referred to as “sudden commencements (SCs)”) first proposed by *Araki* [1977, 1994] separated the magnetic field signatures measured on the ground into components originating from the magnetosphere (i.e., the magnetopause current and the field-aligned currents) and the ionosphere. The sudden increase in the magnetopause current during SIs launches an inward compressional magnetospheric wave that carries a polarization current on the wave front. As the compressional wave propagates inward, it undergoes a mode conversion upon reaching a steep gradient in the Alfvén speed, and this influences the field-aligned currents flowing in and out of the ionosphere. Numerical modeling of the magnetosphere has been shown to well replicate these effects over the few minute time scale that these effects occur [*Fujita et al.*, 2003a, 2003b]. These field-aligned currents set up positive and negative electric potential on the dusk and dawn sectors, respectively, which drives a two-cell Hall current system in the high-latitude ionosphere [e.g., *Kikuchi and Hashimoto*, 2016]. The equatorial ionosphere is effectively connected to the high-latitude two-cell Hall current system via Pederson currents at mid latitudes [see *Araki et al.*, 2009, Figure 1]. As a result, the Cowling effect at the magnetic equator causes a sudden response of the equatorial electrojet (EEJ) to the SI event. Recently, *Piersanti and Villante* [2016] developed a technique to extract the magnetospheric (*DL*) and the ionospheric (*DP*) origin fields from a ground signal during a SI. They evaluated the *DL* field by a comparison between magnetospheric field observations and *Tsyganenko and Sitnov* [2005] model predictions. The *DP* field is extracted by subtracting the estimated *DL* field from ground observations.

In the context of GIC research, the EEJ has been suspected to play a significant role in the generation of GICs at equatorial latitudes during geomagnetic storms, much like the auroral electrojets at high-latitude regions [*Pulkkinen et al.*, 2012; *Ngwira et al.*, 2013; *Moldwin and Tsu*, 2016]. Recently, *Carter et al.* [2015] confirmed that the EEJ caused enhanced GIC activity during SI events. Importantly, their analysis showed that equatorial GIC activity was not limited to geomagnetic storms but was also evident for interplanetary shock arrivals that did not precede geomagnetic activity. While 14 years of SI events were analyzed by *Carter et al.* [2015], the physical mechanism connecting SIs to enhanced equatorial GIC activity was not explored in detail.

In this study, an analysis of the magnetic field variations observed on the ground, and the associated GICs, for the 2015 St. Patrick's Day storm (17–18 March) is presented. Of particular focus are the magnetic field variations observed at the magnetic equator in association with perturbations in the EEJ current caused by

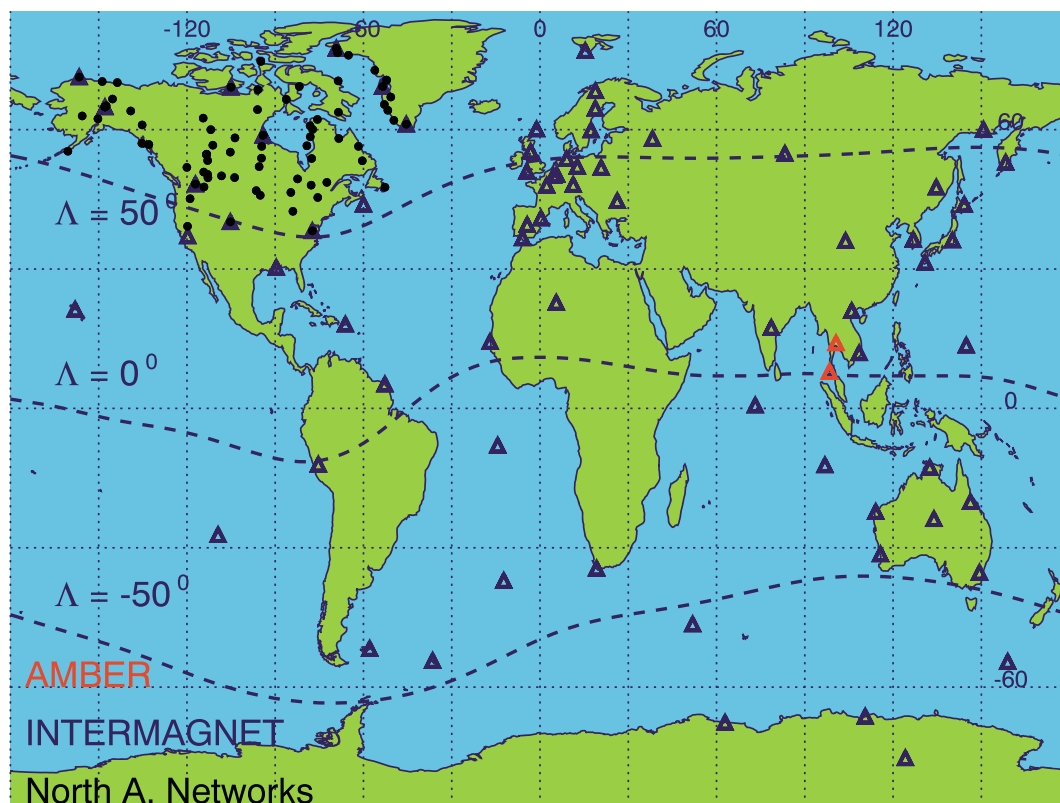


Figure 1. The locations of the INTERMAGNET (blue) and AMBER (orange) magnetometer stations used in this analysis. The black points indicate the locations of North American stations used in a later analysis. The dashed lines indicate the magnetic latitudes 0° and $\pm 50^\circ$.

the storm. High-resolution magnetometer data collected from all over the world allow an investigation into the physical connection between SIs and equatorial GICs.

2. Global Magnetometer Observations

Ground-based magnetometer station data are primarily used in this analysis. Several magnetometer networks exist around the world, and this study uses a subset of them. Due to its global coverage, the International Real-Time Magnetic Observatory Network (INTERMAGNET) [Love and Chulliat, 2013] magnetometer data are predominantly used. This data set is supplemented by the data collected from two Southeast Asian stations in Phuket and Bangkok, which are recent additions to the African Meridian B-Field Education and Research (AMBER) network [Yizengaw and Moldwin, 2009] to extend its longitudinal coverage. The observations collected at the magnetic equator by the AMBER Phuket station are particularly important in this study.

Figure 1 shows the locations of the stations used in this analysis. The blue triangles show the locations of the stations from INTERMAGNET, and the orange triangles are the two chosen stations from the AMBER network. The black dots in the North American region are stations from several networks that include Athabasca University Time History of Events and Macroscale Interactions (THEMIS) UCLA Magnetometer Network (AUTUMNX); Canadian Array for Real time Investigations of Magnetic Activity (CARISMA) [Mann et al., 2008]; Canadian Magnetic Observatory Network (CANMOS); magnetometers in Greenland that are operated by the Technical University of Denmark; Geophysical Institute Magnetometer Array (GIMA); Magnetometer Array for Cusp and Cleft Studies (MACCS) [Engebretson et al., 1995]; Mid-continent MAGnetoseismic Chain (McMAC) [Chi et al., 2013]; the Solar and Terrestrial Physics (STEP) chain; the THEMIS ground magnetometers [Russell et al., 2009], and U.S. Geological Survey (USGS) stations and are used to produce ionospheric current strength information. The dashed lines indicate the locations of the 0° and $\pm 50^\circ$ magnetic latitudes estimated using Baker and Wing's [1989] model.

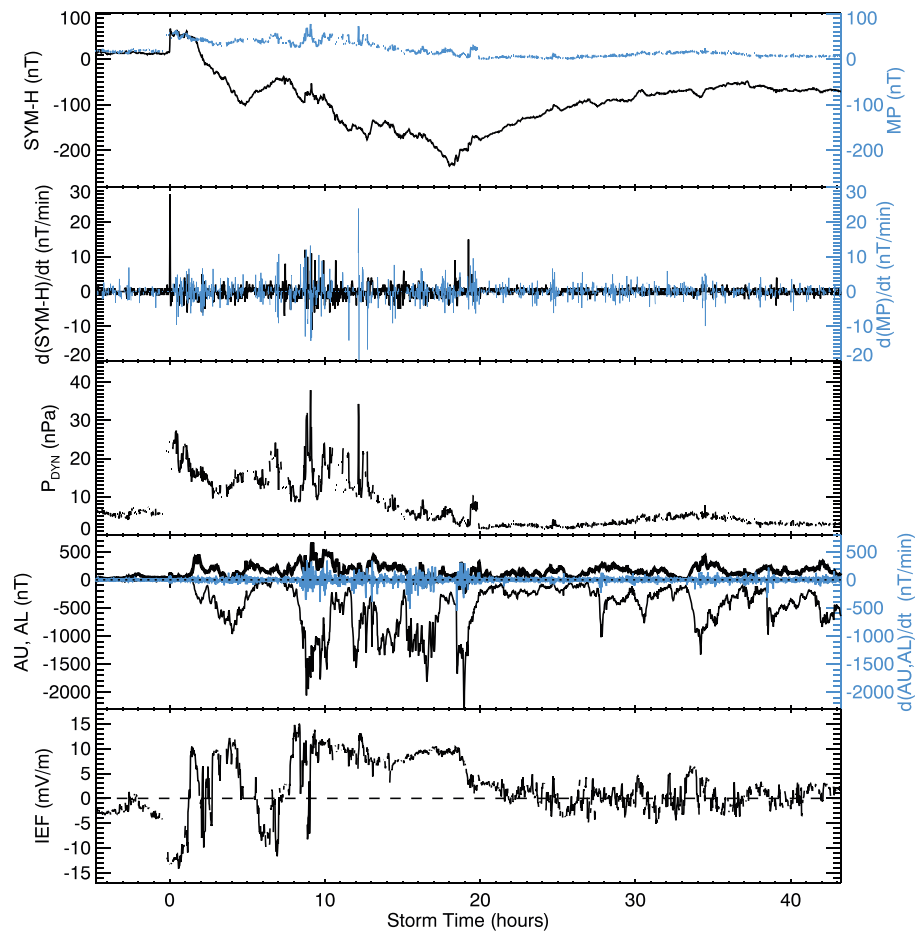


Figure 2. Geomagnetic activity summary for 17 March 2015 storm, including *SYM-H* index and the magnetopause (MP) contribution toward the *SYM-H* index (blue), the temporal variations in the *SYM-H* index and the MP contribution, the solar wind dynamic pressure as calculated using the Wind spacecraft data, the *AU* (thick) and *AL* indices and their temporal variations (blue), and finally the interplanetary electric field also calculated using Wind spacecraft data. The x axis is in storm time, which commences at 0445 UT on 17 March 2015 (i.e., storm time = UT -4.75).

3. Results and Discussion

3.1. Geomagnetic Activity Summary

Before the analysis of the magnetometer data, a brief overview of the 17–18 March 2015 storm is given. Figure 2, from the top panel to the bottom, shows the *SYM-H* index and the contribution of the magnetopause (MP) current to the *SYM-H* index (blue); the temporal changes in the *SYM-H* index and the MP current contribution (blue); the solar wind dynamic pressure measured by the Wind spacecraft, shifted in time to the bow shock; the *AU* (thick) and *AL* (thin) indices and their temporal variations (blue); and finally the interplanetary electric field (IEF = $-V \times B_2$) calculated from Wind data, which has also been shifted to the bow shock. The MP current contribution to the *SYM-H* index has been calculated in the same way as Carter *et al.* [2015], using the empirical formula given by Burton *et al.* [1975] and Gonzalez *et al.* [1994]. The time axis is storm time taken from 0445 UT on 17 March 2015, which is when the initial interplanetary shock arrived (i.e., storm time = UT -4.75). The *AU* and *AL* indices use magnetometer data from several auroral-latitude stations to quantify the eastward and westward auroral electrojet activities, respectively [Kamide and Akasofu, 1983], and are used as a simple indicator of substorm activity in this study.

At the storm sudden commencement (SSC, 0445 UT on 17 March 2015), there is an abrupt increase in the *SYM-H* index that coincides with the initial interplanetary shock in the solar wind dynamic pressure. The change in the *SYM-H* index is close to 30 nT/min. For this feature there is a gap in the solar wind data, but the data shortly after the shock show that the MP current has substantially increased as a result of this

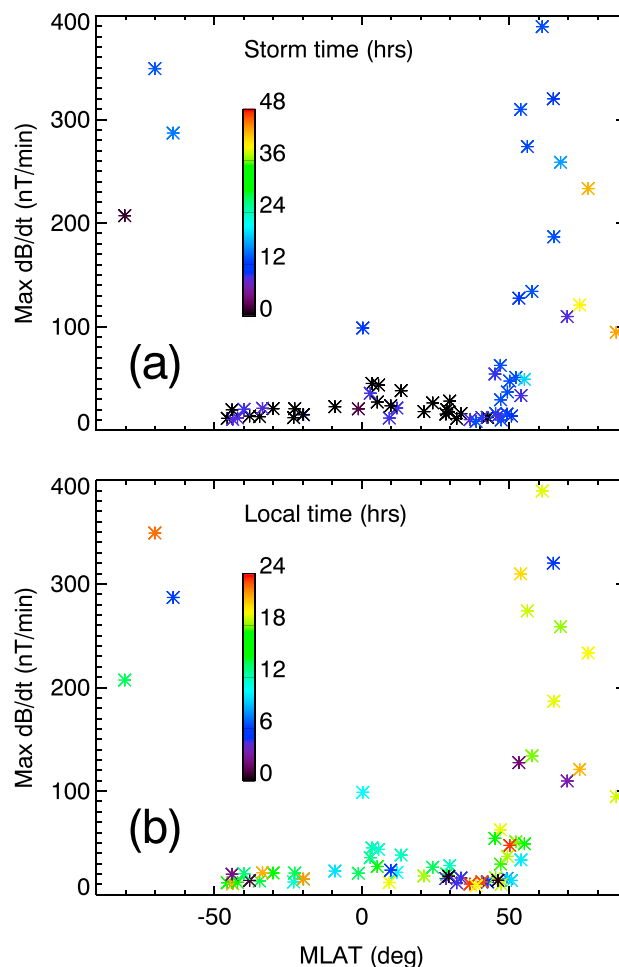


Figure 3. (a) Maximum dB/dt as a function of magnetic latitude using 1 min magnetometer data, colored according to the number of hours into the storm when the maximum dB/dt was measured. (b) Same as Figure 3a but colored according to the local time at the station when the maximum dB/dt was measured.

which the plotted dB/dt value was observed during the storm, and in Figure 3b the points are colored according to the corresponding local time of the station. First, it is worthwhile to note that the latitudinal distribution of maximum dB/dt , with substantially larger values at latitudes higher than 50° , is similar to those reported in the past for combined storms [e.g., Ngwira et al., 2013; Love et al., 2016], and for individual storms [Pulkkinen et al., 2012].

Interestingly, the maximum dB/dt values in Figure 3a correspond to three groupings in terms of the storm time: (1) black points that correspond to the SSC, (2) blue points that correspond to ~ 10 h into storm, and (3) yellow/red points that correspond to ~ 40 h into the storm. The middle- and low-latitude stations primarily compose group (1), whereas the high-latitude and one equatorial station compose group (2). The third grouping that corresponds to ~ 40 h after SSC consists of stations in the highest latitude locations in the Northern Hemisphere.

Figure 3b also shows some noteworthy groupings: (1) stations measuring their largest dB/dt during the late evening/early morning hours, which are predominantly in the high-latitude regions, and (2) stations measuring their maximum dB/dt values during the local daytime hours, which are predominantly located at middle-to-equatorial latitudes.

Together, Figures 2 and 3 provide indications about which phases of the St. Patrick's Day storm were the most favorable for GIC generation. The low- and middle-latitude stations were most vulnerable to GICs at

shock arrival; the $SYM-H$ increase at SSC is almost fully accounted for by the MP current contribution. The storm's entire main phase lasted approximately 18 h, followed by a recovery phase that lasted at least 25 h.

The $SYM-H$ index and the MP current contribution show several temporal fluctuations during the storm's main phase, some of which coincide well with several abrupt changes in the solar wind dynamic pressure. The AU and AL indices do not become large until close to 9 h after SSC. Importantly, it is also during a period of high substorm activity that the largest variations in the AL index were observed, some reaching close to 500 nT/min. Finally, the IEF data show periods where penetration electric fields are expected to influence ionospheric plasma drifts in both high-latitude and equatorial regions. In particular, crossings from negative IEF to positive IEF indicate interplanetary magnetic field B_z crossings from northward to southward, and thus prompt-penetration electric fields (PPEFs), which are known to influence equatorial ionospheric plasma drifts [e.g., Fejer et al., 2008; Tsurutani et al., 2008; Abdu, 2012].

3.2. Global Magnetic Field Fluctuations

Figure 3 shows the largest temporal variation in the magnetic field, dB/dt , as a function of magnetic latitude for the 17–18 March 2015 storm. In Figure 3a, the points are colored according to the storm time at

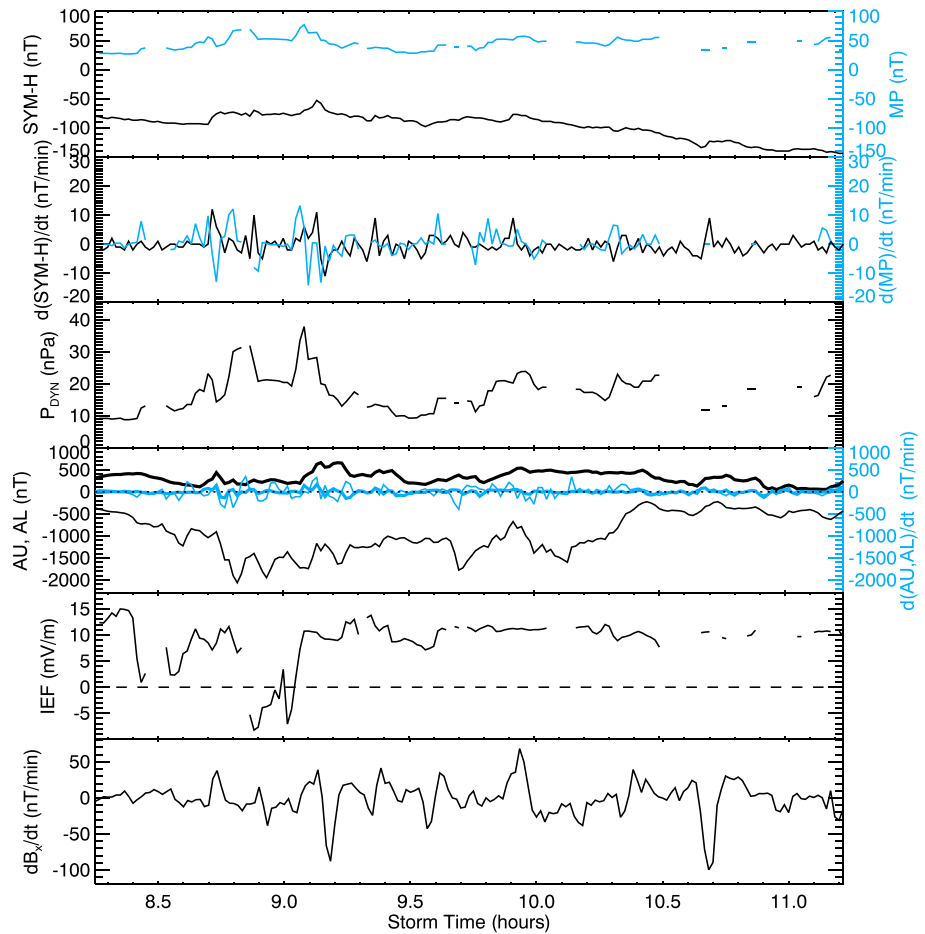


Figure 4. Similar to Figure 2 but between approximately 8.5 and 11 h after storm commencement. The sixth panel shows the time series of dB_x/dt measured by the equatorial station HUA.

the moment of SSC, whereas both the equatorial latitude and high-latitude locations were most susceptible during the elevated auroral electrojet/substorm activity some 10 h into the storm. In the context of space weather prediction for power grid operators, these timings are important and provide a demonstration that forecasting severe substorms [e.g., *Tsurutani et al., 2015*] is important for predicting large GIC events. In terms of the low- and middle-latitude stations, the solar wind data from the Lagrange point L1 are vital for accurately forecasting the arrival time of the storms' initial shock (i.e., the SSC), and also, their severity in terms of dB/dt on the ground, which can be estimated using the solar wind dynamic pressure observations, see Figure 2.

3.3. Equatorial GICs in South America

Given that many studies have investigated the generation mechanisms of severe GICs in high-latitude regions, we focus our attention to the largest dB/dt values observed in the equatorial region, particularly those observed by the station at Huancayo, Peru (HUA); the point of $dB/dt \approx 100$ nT/min at 0° in Figure 3. Figure 4 shows the time series of the geomagnetic summary presented in Figure 2, but between 13 and 16 UT (between approximately 8 and 11 h storm time). During this interval, HUA observed its largest dB/dt values predominantly in the x direction (i.e., northward), which are displayed in Figure 4 (sixth panel).

The largest dB/dt value plotted from HUA in Figure 3 corresponds to the negative dB_x/dt spike at 10.7 h after SSC in Figure 4. At this time, unfortunately, there is a gap in the solar wind data, which complicates efforts to understand what role, if any, the solar wind played in this equatorial dB/dt enhancement. Fortunately, another large dB/dt perturbation occurred at 9.2 h after SSC; a time when the solar wind data are complete. This dB/dt spike was largest at 9.2 h after SSC, but it began close to 9.1 h when abrupt increases in both the solar wind dynamic pressure and the SYM-H index were observed. There is a notable time difference between the SYM-H increase and the solar wind dynamic pressure increase at e. 9.1 h, but this difference is most likely due to a

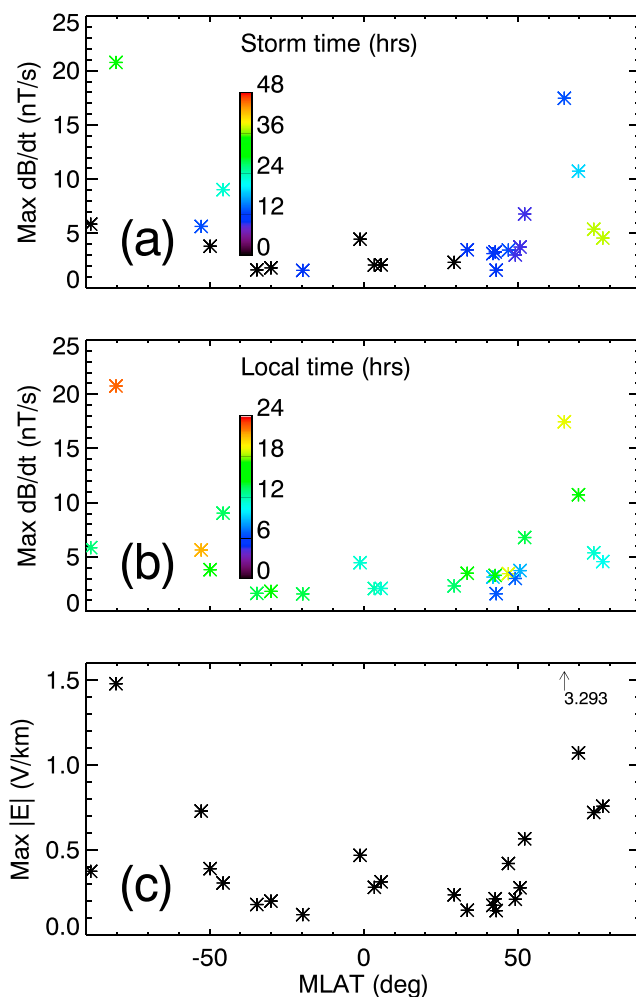


Figure 5. (a, b) Similar to Figure 3 but using 1 s magnetometer data. (c) The calculated geoelectric field for each station versus magnetic latitude.

slight inaccuracy in the propagation of the solar wind data to the bow shock. Another indication of a slight propagation inaccuracy is the fact that the $d(SYM-H)/dt$ and $d(MP)/dt$ spikes observed close to 9.1 h are similar in magnitude, but slightly shifted. A brief correlation analysis found that the highest correlation was achieved by delaying the solar wind data by a further 4 min.

Importantly, just before the moment of the HUA spike at 9.2 h after SSC, the IEF shifts from negative to positive and is a prime moment for an eastward directed PPEF at the equator on the dayside. When acting alone, such an electric field would enhance the equatorial electrojet in the eastward direction and $\vec{E} \times \vec{B}$ drift the ionospheric plasma vertically at the equator on the dayside [e.g., Fejer et al., 2008; Tsurutani et al., 2008]. In the magnetometer data, this would correspond to a sudden increase in the northward component of the magnetic field due to an eastward enhancement in the EEJ strength above that location in response to the PPEF. However, a sudden decrease in the northward magnetic field is shown in Figure 4. The increase in the B_x just prior to the negative excursion may indeed be due to the PPEF, but the negative excursion itself is simply in the wrong direction to be caused by the PPEF in this instance.

In order to better understand how enhanced dB/dt activity at the magnetic equator can be related to sudden changes in the solar wind dynamic pressure, we later shift our focus to the SSC at 0445 UT on 17 March, before other magnetosphere and ionosphere current systems had the chance to develop; such as ring current and the counterelectrojet current. While some previous studies have researched SSCs with 1 min resolution data [e.g., Carter et al., 2015], the high-frequency variations during SSCs are much better captured using 1 s resolution.

3.4. Equatorial GICs at Storm Sudden Commencement

Figures 5a and 5b are the same as Figures 3a and 3b, but 1 s data are used, for the stations where it was available. Overall, these figures exhibit similar features to Figures 3a and 3b. Stations at higher latitudes than 50° exhibit much higher dB/dt than lower latitude stations, and these larger dB/dt variations correspond to times when significant auroral activity was present, as discussed earlier. Figure 5c shows the geoelectric field calculated from the 1 s magnetometer data in the same manner as Pulkkinen et al. [2012]. It can be seen that geoelectric fields got as high as 3.3 V/km in the high-latitude regions and 0.5 V/km in the equatorial region. The overall latitudinal pattern is similar to the 1 min data presented in Figure 3.

One subtle difference between Figures 5a and 3a is the timing of the equatorial peak, i.e., 10.7 h after SSC in Figure 3a versus at the moment of SSC in Figure 5a. The peak in Figure 5a actually comes from the equatorial AMBER station, PUKT (orange triangle on the magnetic equator in Figure 1). It should be noted that HUA did

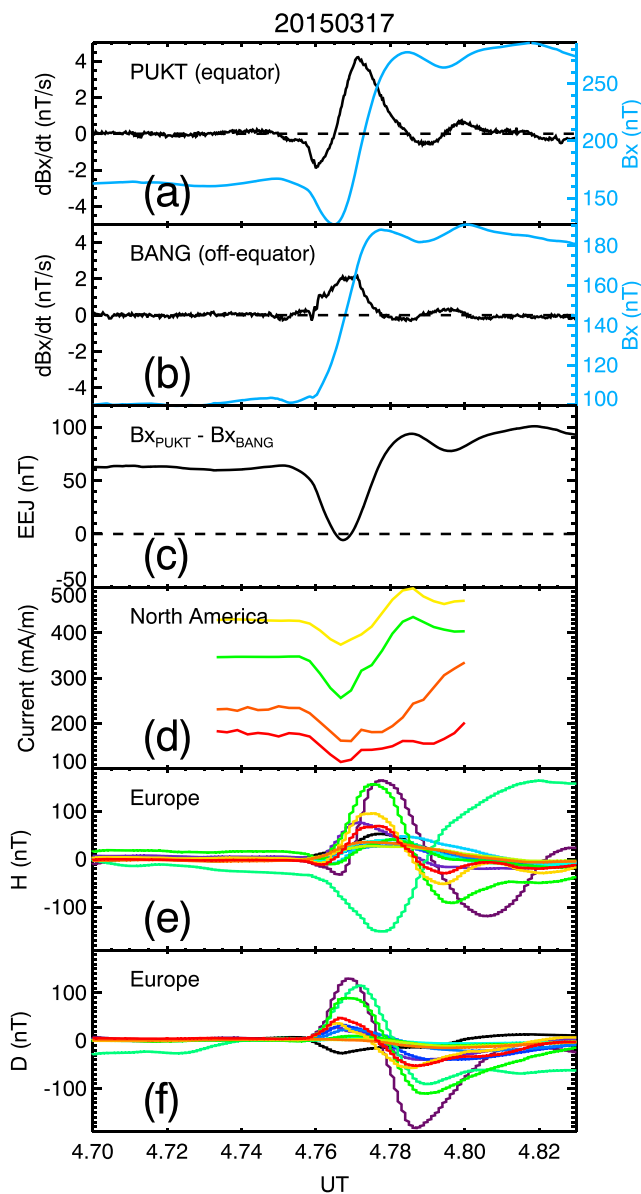


Figure 6. (a, b) The dB_x/dt data for PUKT and BANG stations during the SSC event on 17 March 2015. The blue lines show the B_x data for each station. (c) The difference between the B_x measured by PUKT and BANG, or effectively the EEJ strength, as a function of time. (d) The ionospheric current magnitudes for four selected locations across North America, see text for details. (e) The contribution of the ionospheric current to the H component (northward) measured by several magnetometers located across Europe and North Africa. (f) The same as Figure 6e but for the D component (eastward).

data indicate that the largest dB/dt at the equator originates from the sudden increase in the EEJ strength following its initial drop to 0 nT.

3.5. Ionospheric Current Response to SSC at High and Equatorial Latitudes

While Carter *et al.* [2015] connected the interplanetary shock arrivals to increased GIC activity at the equator, the physical mechanism was not explored in detail. The high-resolution magnetometer data available for the 17 March 2015 storm allows such an exploration in this instance. As mentioned earlier, many previous studies have investigated the global magnetic field signatures of interplanetary shock arrivals [e.g., Araki, 1977, 1994;

not have 1 s data available for this event, hence why it is missing from this plot. This equatorial enhancement at SSC presents a significant opportunity to investigate the physical mechanism behind the enhancement of GIC activity at the magnetic equator.

Figures 6a and 6b show the time series of the dB_x/dt at the moment of SSC for the PUKT (equatorial station) and BANG (off-equatorial station). The B_x component for each station is overplotted. The maximum dB_x/dt measured by PUKT is approximately twice that measured by BANG. Interestingly, the PUKT data also show a negative deviation prior to the main pulse, but the off-equatorial station BANG only observed a positive dB_x/dt spike. As shown in Figure 1, these two AMBER stations are close to each other and should therefore measure similar magnetic field variations, with the obvious exception of those caused by the EEJ current, which only PUKT is close enough to measure. This magnetometer configuration has been used extensively in the past in order to isolate the magnetic field fluctuations caused by the EEJ [e.g., Anderson *et al.*, 2002; Yizengaw *et al.*, 2012, 2014]. The basic idea is to simply take the difference in the strength of the B_x component measured off the equator from the B_x component measured at the equator, and the difference is taken to be due to the EEJ.

Figure 6c shows this difference during the SSC. Prior to the SSC, the EEJ is steady at approximately 65 nT. At the moment of the SSC the EEJ abruptly drops to near 0 nT and then rises to almost 100 nT. A small decrease to ~ 80 nT then occurs, followed by a gentle increase up toward 100 nT. These

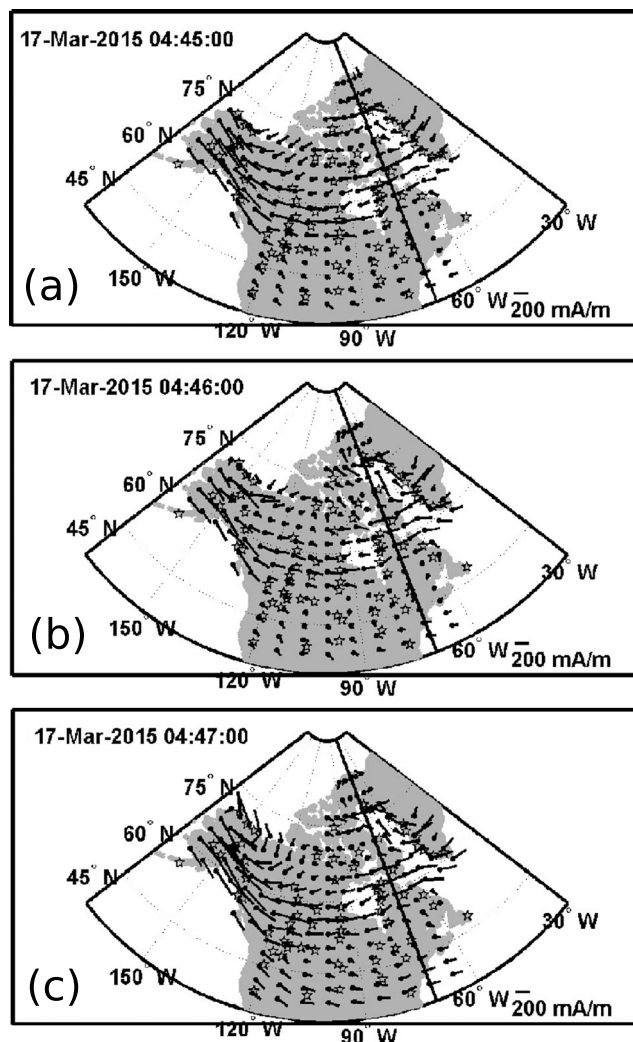


Figure 7. (a–c) The ionospheric current vector fields across North America using the spherical elementary current systems method [Amm and Viljanen, 1999; Weygand et al., 2011] for 0445 UT, 0446 UT, and 0447 UT on 17 March 2015. The solid line indicates the longitude of local midnight.

ionospheric current strength significantly decreased and then increased to a stronger eastward current in response to the SSC. Interestingly, this auroral current variation is similar to, and coincides with, the EEJ strength above Southeast Asia, see Figure 6c, despite the large distance between these phenomena.

The ionospheric current above the European (dawn) sector is also investigated by the use of the Piersanti and Villante [2016] technique for the extraction of the *DP* fields from ground magnetometer observations. The ionospheric contributions toward the magnetic field in the northward and eastward directions as measured by the magnetometers across Europe and northern Africa is plotted in Figures 6e and 6f, respectively. Each color represents a separate station. The first feature worth noting is that the majority of stations measure a sudden increase in the northward component of the magnetic field, which corresponds to an increase in the auroral electrojet in the eastward direction at the moment of SSC. A high-latitude station actually observes the opposite. One more interesting feature is the slight delay between the response observed in the European sector compared to the Southeast Asian equatorial region and the North American region.

According to Araki, 's [1977, 1994] model for SSC, a two-cell Hall current system forms in the high-latitude region; one cell each in the morning and evening sectors. The evening cell effectively connects the auroral region to the equatorial region, and as such, the changes in the evening auroral electrojet and equatorial

Araki et al., 2009; Shinbori et al., 2009, and references therein]. The data sets available for this analysis facilitate a direct comparison between the high-latitude ionospheric currents in both dusk and dawn hemispheres, in addition to the dayside EEJ.

To investigate how the major ionospheric current systems responded to the 17 March 2015 SSC, both ionospheric current strengths in the North American and European regions are analyzed.

The major ionospheric currents systems over North America are calculated using the spherical elementary current systems method [Amm and Viljanen, 1999; Weygand et al., 2011]. This technique uses singular value decomposition to invert the ground magnetometer magnetic field fluctuations and determine the ionospheric current system. Figures 7a–7c show the ionospheric current strength vectors across North America using this technique at 0445, 0446, and 0447 UT on 17 March 2015, respectively. These figures show that there was a reduction in the ionospheric current strength from 0445 UT to 0446 UT, followed by a recovery at 0447 UT. This reduction in ionospheric current strength is most obvious over the Alaskan/Western Canadian regions. Figure 6d shows the time series of the ionospheric current amplitudes in the North American (dusk) sector for four locations; (61.9°N, 120.3°W), (59.0°N, 120.3°W), (61.9°N, 147.9°W), and (61.9°N, 141.0°W). The eastward

electrojet currents due to the SSC should have the same polarity. The morning sector cell, which is not connected to the dayside equatorial region, has the opposite polarity and thus has the opposite SSC response. Overall, the SSC model described by Araki [1977, 1994] appears to be well supported by the observations reported here. At the moment of SSC the auroral electrojet in the evening sector and the dayside EEJ experience a sharp westward surge, followed by another abrupt eastward enhancement to above pre-SSC levels. This observation suggests a conductive link between the evening auroral electrojet and the equatorial electrojet in response to the field-aligned currents generated by the interplanetary shock arrival at SSC. In the morning sector, however, the opposite is observed; a sudden increase in the eastward auroral electrojet followed by a return to pre-SSC levels. A more complete picture of the physics in SSCs could be obtained from global field-aligned current maps, for example, those provided by AMPERE (Active Magnetospheric and Planetary Electrodynamics Response Experiment) [Anderson *et al.*, 2000]; however, fully capturing the spatial and temporal variations during SSCs is a significant challenge.

4. Summary and Conclusions

In this study, the GICs caused by the 17–18 March 2015 storm, the largest so far in the current solar cycle, were examined. The largest magnetic field variations were observed in the high-latitude regions approximately 10 h after the storm's commencement. At middle and low latitudes, however, the magnetic field variations were reduced compared to those at high latitudes, but they occurred at the moment of the SSC, predominantly on the dayside. At equatorial latitudes, enhanced GIC activity was observed both at the moment of SSC and approximately 10 h into the storm, at similar times to the largest perturbations in the high-latitude regions. Our analysis of both instances of high GIC activity at the equator suggests that the magnetospheric and ionospheric current perturbations associated with a sudden increase in solar wind dynamic pressure were responsible and that prompt-penetration electric fields only played a subsidiary role. A comparison between the EEJ and auroral electrojet strengths in both the morning and evening sectors supports Araki [1977, 1994]'s model for SSCs.

Acknowledgments

This research was partially supported by the Australian Research Council Linkage (LP130100243) and National Science Foundation (AGS1265651 and AGS1450512) grants. The results presented in this paper rely on data collected at magnetic observatories. We thank the national institutes that support them and INTERMAGNET for promoting high standards of magnetic observatory practice (www.intermagnet.org). The geomagnetic activity and solar wind data were obtained from NASA's OMNIWeb online facility (<http://omniweb.gsfc.nasa.gov/>). The authors would also like to acknowledge the open magnetometer data policies of AUTUMNX (<http://autumn.athabascau.ca/>), CARISMA, CANMOS (<http://gsc.nrcan.gc.ca/geomag/>), the Technical University of Denmark (http://www.hspace.dtu.dk/english/Research/Scientific_data_and_models/Magnetic_Ground_Stations/), GIMA (<http://magnet.gi.alaska.edu/>), MACCS, McMAC, STEP (maintained by Dr. Kanji Hayashi, hayashi@grl.s.u-tokyo.ac.jp, <http://step-p.dyndns.org/~khay/>), THEMIS, and the USGS (<http://geomag.usgs.gov>).

References

- Abdu, M. A. (2012), Equatorial spread F /plasma bubble irregularities under storm time disturbance electric fields, *J. Atmos. Sol. Terr. Phys.*, *75*–76, 44–56.
- Amm, O., and A. Viljanen (1999), Ionospheric disturbance magnetic field continuation from the ground to the ionosphere using spherical elementary current systems, *Earth Planets Space*, *51*, 431–440.
- Anderson, B. J., K. Takahashi, and B. A. Toth (2000), Sensing global Birkeland currents with iridium® engineering magnetometer data, *Geophys. Res. Lett.*, *27*(24), 4045–4048, doi:10.1029/2000GL000094.
- Anderson, D., A. Anghel, K. Yumoto, M. Ishitsuka, and E. Kudeki (2002), Estimating daytime vertical $E \times B$ drift velocities in the equatorial F -region using ground-based magnetometer observations, *Geophys. Res. Lett.*, *29*(12), 1596, doi:10.1029/2001GL014562.
- Araki, T. (1977), Global structure of geomagnetic sudden commencements, *Planet. Space Sci.*, *25*, 373–384.
- Araki, T. (1994), *A physical model of the geomagnetic sudden commencement*, pp. 183–200, AGU, Washington, D. C., doi:10.1029/GM081p0183.
- Araki, T., S. Tsunomura, and T. Kikuchi (2009), Local time variation of the amplitude of geomagnetic sudden commencements (SC) and SC-associated polar cap potential, *Earth Planets Space*, *61*, e13–e16.
- Astafeyeva, E., I. Zakharenkova, and M. Förster (2015), Ionospheric response to the 2015 St. Patrick's Day storm: A global multi-instrumental overview, *J. Geophys. Res. Space Physics*, *120*, 9023–9037, doi:10.1002/2015JA021629.
- Baker, K. B., and S. Wing (1989), A new magnetic coordinate system for conjugate studies at high latitudes, *J. Geophys. Res.*, *94*(A7), 9139–9143, doi:10.1029/JA094iA07p09139.
- Burton, R. K., R. L. McPherron, and C. T. Russell (1975), An empirical relationship between interplanetary conditions and *Dst*, *J. Geophys. Res.*, *80*(31), 4204–4214, doi:10.1029/JA080i031p04204.
- Carter, B. A., E. Yizengaw, R. Pradipta, A. J. Halford, R. Norman, and K. Zhang (2015), Interplanetary shocks and the resulting geomagnetically induced currents at the equator, *Geophys. Res. Lett.*, *42*, 6554–6559, doi:10.1002/2015GL065060.
- Carter, B. A., E. Yizengaw, R. Pradipta, J. M. Retterer, K. Groves, C. Valladares, R. Caton, C. Bridgwood, R. Norman, and K. Zhang (2016), Global equatorial plasma bubble occurrence during the 2015 St. Patrick's Day storm, *J. Geophys. Res. Space Physics*, *121*, 894–905, doi:10.1002/2015JA022194.
- Chi, P. J., et al. (2013), Sounding of the plasmasphere by Mid-continent MAGnetoseismic Chain (McMAC) magnetometers, *J. Geophys. Res. Space Physics*, *118*, 3077–3086, doi:10.1002/jgra.50274.
- Engelbreton, M. J., W. J. Hughes, J. L. Alford, E. Zesta, L. J. Cahill, R. L. Arnoldy, and G. D. Reeves (1995), Magnetometer array for cusp and cleft studies observations of the spatial extent of broadband ULF magnetic pulsations at cusp/cleft latitudes, *J. Geophys. Res.*, *100*(A10), 19,371–19,386, doi:10.1029/95JA00768.
- Fagundes, P. R., F. A. Cardoso, B. G. Fejer, K. Venkatesh, B. A. G. Ribeiro, and V. G. Pillat (2016), Positive and negative GPS-TEC ionospheric storm effects during the extreme space weather event of March 2015 over the Brazilian sector, *J. Geophys. Res. Space Physics*, *121*, 5613–5625, doi:10.1002/2015JA022214.
- Fejer, B. G., J. W. Jensen, and S.-Y. Su (2008), Seasonal and longitudinal dependence of equatorial disturbance vertical plasma drifts, *Geophys. Res. Lett.*, *35*, L21016, doi:10.1029/2008GL035584.
- Fiori, R. A. D., D. H. Boteler, and D. M. Gillies (2014), Assessment of GIC risk due to geomagnetic sudden commencements and identification of the current systems responsible, *Space Weather*, *12*, 76–91, doi:10.1002/2013SW000967.

- Forbes, K. F., and O. C. St. Cyr (2008), Solar activity and economic fundamentals: Evidence from 12 geographically disparate power grids, *Space Weather*, *6*, S10003, doi:10.1029/2007SW000350.
- Fujita, S., T. Tanaka, T. Kikuchi, K. Fujimoto, K. Hosokawa, and M. Itonaga (2003a), A numerical simulation of the geomagnetic sudden commencement: 1. Generation of the field-aligned current associated with the preliminary impulse, *J. Geophys. Res.*, *108*(A12), 1416, doi:10.1029/2002JA009407.
- Fujita, S., T. Tanaka, T. Kikuchi, K. Fujimoto, and M. Itonaga (2003b), A numerical simulation of the geomagnetic sudden commencement: 2. Plasma processes in the main impulse, *J. Geophys. Res.*, *108*(A12), 1417, doi:10.1029/2002JA009763.
- Gaunt, C. T. (2016), Why space weather is relevant to electrical power systems, *Space Weather*, *14*(1), 2–9, doi:10.1002/2015SW001306.
- Gonzalez, W. D., J. A. Joselyn, Y. Kamide, H. W. Kroehl, G. Rostoker, B. T. Tsurutani, and V. M. Vasyliunas (1994), What is a geomagnetic storm?, *J. Geophys. Res.*, *99*, 5771–5792, doi:10.1029/93JA02867.
- Huang, C.-S., G. R. Wilson, M. R. Hairston, Y. Zhang, W. Wang, and J. Liu (2016), Equatorial ionospheric plasma drifts and O⁺ concentration enhancements associated with disturbance dynamo during the 2015 St. Patrick's Day magnetic storm, *J. Geophys. Res. Space Physics*, *121*, 7961–7973, doi:10.1002/2016JA023072.
- Joshi, L. M., S. Sripathi, and R. Singh (2016), Simulation of low-latitude ionospheric response to 2015 St. Patrick's Day super geomagnetic storm using ionosonde-derived PRE vertical drifts over Indian region, *J. Geophys. Res. Space Physics*, *121*, 2489–2502, doi:10.1002/2015JA021512.
- Kakad, B., P. Gurrum, P. N. B. Tripura Sundari, and A. Bhattacharyya (2016), Structuring of intermediate scale equatorial spread *F* irregularities during intense geomagnetic storm of solar cycle 24, *J. Geophys. Res. Space Physics*, *121*, 7001–7012, doi:10.1002/2016JA022635.
- Kamide, Y., and S.-I. Akasofu (1983), Notes on the auroral electrojet indices, *Rev. Geophys.*, *21*(7), 1647–1656, doi:10.1029/RG021i007p01647.
- Kappenman, J. G. (2003), Storm sudden commencement events and the associated geomagnetically induced current risks to ground-based systems at low-latitude and midlatitude locations, *Space Weather*, *1*(3), 1016, doi:10.1029/2003SW000009.
- Kappenman, J. G. (2005), An overview of the impulsive geomagnetic field disturbances and power grid impacts associated with the violent Sun-Earth connection events of 29–31 October 2003 and a comparative evaluation with other contemporary storms, *Space Weather*, *3*, S08C01, doi:10.1029/2004SW000128.
- Kikuchi, T., and K. K. Hashimoto (2016), Transmission of the electric fields to the low latitude ionosphere in the magnetosphere-ionosphere current circuit, *Geosci. Lett.*, *3*(1), 1–11, doi:10.1186/s40562-016-0035-6.
- Knipp, D. J. (2015), Synthesis of geomagnetically induced currents: Commentary and research, *Space Weather*, *13*(11), 727–729, doi:10.1002/2015SW001317.
- Love, J. J., and A. Chulliat (2013), An international network of magnetic observatories, *Eos Trans. AGU*, *94*(42), 373–374, doi:10.1002/2013EO420001.
- Love, J. J., P. Coisson, and A. Pulkkinen (2016), Global statistical maps of extreme-event magnetic observatory 1 min first differences in horizontal intensity, *Geophys. Res. Lett.*, *43*, 4126–4135, doi:10.1002/2016GL068664.
- Mann, I. R., et al. (2008), The upgraded CARISMA magnetometer array in the THEMIS era, *Space Sci. Rev.*, *141*(1), 413–451, doi:10.1007/s11214-008-9457-6.
- Marshall, R. A., E. A. Smith, M. J. Francis, C. L. Waters, and M. D. Sciffer (2011), A preliminary risk assessment of the Australian region power network to space weather, *Space Weather*, *9*, S10004, doi:10.1029/2011SW000685.
- Marshall, R. A., M. Dalzell, C. L. Waters, P. Goldthorpe, and E. A. Smith (2012), Geomagnetically induced currents in the New Zealand power network, *Space Weather*, *10*, S08003, doi:10.1029/2012SW000806.
- Schulte in den Bäumen, H., D. Moran, M. Lenzen, I. Cairns, and A. Steenge (2014), How severe space weather can disrupt global supply chains, *Nat. Hazards Earth Syst. Sci.*, *14*, 2749–2759, doi:10.5194/nhess-14-2749-2014.
- Moldwin, M. B., and J. S. Tsu (2016), *Stormtime Equatorial Electrojet Ground Induced Currents: Increasing Power Grid Space Weather Impacts at Equatorial Latitudes*, Chapter 3, AGU, Washington, D. C.
- Ngwira, C. M., A. Pulkkinen, F. D. Wilder, and G. Crowley (2013), Extended study of extreme geoelectric field event scenarios for geomagnetically induced current applications, *Space Weather*, *11*, 121–131, doi:10.1002/swe.20021.
- Piersanti, M., and U. Villante (2016), *J. Geophys. Res. Space Physics*, *121*, 6674–6691, doi:10.1002/2015JA021666.
- Pirjola, R. (2000), Geomagnetically induced currents during magnetic storms, *IEEE Trans. Plasma Sci.*, *28*(6), 1867–1873, doi:10.1109/27.902215.
- Pulkkinen, A., S. Lindahl, A. Viljanen, and R. Pirjola (2005), Geomagnetic storm of 29–31 October 2003: Geomagnetically induced currents and their relation to problems in the Swedish high-voltage power transmission system, *Space Weather*, *3*, S08C03, doi:10.1029/2004SW000123.
- Pulkkinen, A., E. Bernabeu, J. Eichner, C. Beggan, and A. W. P. Thomson (2012), Generation of 100-year geomagnetically induced current scenarios, *Space Weather*, *10*, S04003, doi:10.1029/2011SW000750.
- Ramsingh, S. Sripathi, S. Sree Kumar, S. Banola, K. Emperumal, P. Tiwari, and B. S. Kumar (2015), Low-latitude ionosphere response to super geomagnetic storm of 17/18 March 2015: Results from a chain of ground-based observations over Indian sector, *J. Geophys. Res. Space Physics*, *120*, 10,864–10,882, doi:10.1002/2015JA021509.
- Russell, C. T., M. Ginskey, and S. M. Petrinec (1994), Sudden impulses at low-latitude stations: Steady state response for northward interplanetary magnetic field, *J. Geophys. Res.*, *99*(A1), 253–261, doi:10.1029/93JA02288.
- Russell, C. T., P. J. Chi, D. J. Dearborn, Y. S. Ge, B. Kuo-Tiong, J. D. Means, D. R. Pierce, K. M. Rowe, and R. C. Snare (2009), *THEMIS ground-based magnetometers*, pp. 389–412, Springer, New York, doi:10.1007/978-0-387-89820-9_17.
- Schrijver, C. J., R. Dobbins, W. Murtagh, and S. M. Petrinec (2014), Assessing the impact of space weather on the electric power grid based on insurance claims for industrial electrical equipment, *Space Weather*, *12*, 487–498, doi:10.1002/2014SW001066.
- Shinbori, A., Y. Tsuji, T. Kikuchi, T. Araki, and S. Watari (2009), Magnetic latitude and local time dependence of the amplitude of geomagnetic sudden commencements, *J. Geophys. Res.*, *114*, A04217, doi:10.1029/2008JA013871.
- Trivedi, N. B., et al. (2007), Geomagnetically induced currents in an electric power transmission system at low latitudes in Brazil: A case study, *Space Weather*, *5*, S04004, doi:10.1029/2006SW000282.
- Tsurutani, B. T., et al. (2008), Prompt Penetration Electric Fields (PPEFs) and their ionospheric effects during the great magnetic storm of 30–31 October 2003, *J. Geophys. Res.*, *113*, A05311, doi:10.1029/2007JA012879.
- Tsurutani, B. T., R. Hajra, E. Echer, and J. W. Gjerloev (2015), Extremely intense (SML \leq -2500 nT) substorms: Isolated events that are externally triggered?, *Ann. Geophys.*, *33*(5), 519–524, doi:10.5194/angeo-33-519-2015.
- Tsyganenko, N. A., and M. I. Sitnov (2005), Modeling the dynamics of the inner magnetosphere during strong geomagnetic storms, *J. Geophys. Res.*, *110*, A03208, doi:10.1029/2004JA010798.
- Tulasi Ram, S., et al. (2016), Duskside enhancement of equatorial zonal electric field response to convection electric fields during the St. Patrick's day storm on 17 March 2015, *J. Geophys. Res. Space Physics*, *121*, 538–548, doi:10.1002/2015JA021932.

- Viljanen, A. (1998), Relation of geomagnetically induced currents and local geomagnetic field variations, *IEEE Trans. Power Delivery*, *13*(4), 1285–1290.
- Watari, S., et al. (2009), Measurements of geomagnetically induced current in a power grid in Hokkaido, Japan, *Space Weather*, *7*, S03002, doi:10.1029/2008SW000417.
- Weygand, J. M., O. Amm, A. Viljanen, V. Angelopoulos, D. Murr, M. J. Engebretson, H. Gleisner, and I. Mann (2011), Application and validation of the spherical elementary currents systems technique for deriving ionospheric equivalent currents with the North American and Greenland ground magnetometer arrays, *J. Geophys. Res.*, *116*, A03305, doi:10.1029/2010JA016177.
- Yizengaw, E., and M. B. Moldwin (2009), African Meridian B-Field Education and Research (AMBER) array, *Earth Moon Planets*, *104*(1), 237–246, doi:10.1007/s11038-008-9287-2.
- Yizengaw, E., E. Zesta, M. B. Moldwin, B. Damtie, A. Mebrahtu, C. E. Valladares, and R. F. Pfaff (2012), Longitudinal differences of ionospheric vertical density distribution and equatorial electrodynamics, *J. Geophys. Res.*, *117*, A07312, doi:10.1029/2011JA017454.
- Yizengaw, E., M. B. Moldwin, E. Zesta, C. M. Biouele, B. Damtie, A. Mebrahtu, B. Rabiou, C. F. Valladares, and R. Stoneback (2014), The longitudinal variability of equatorial electrojet and vertical drift velocity in the African and American sectors, *Ann. Geophys.*, *32*(3), 231–238, doi:10.5194/angeo-32-231-2014.
- Zhang, J. J., C. Wang, T. R. Sun, C. M. Liu, and K. R. Wang (2015), GIC due to storm sudden commencement in low-latitude high-voltage power network in China: Observation and simulation, *Space Weather*, *13*(10), 643–655, doi:10.1002/2015SW001263.
- Zhang, J. J., C. Wang, T. R. Sun, and Y. D. Liu (2016), Risk assessment of the extreme interplanetary shock of 23 July 2012 on low-latitude power networks, *Space Weather*, *14*(3), 259–270, doi:10.1002/2015SW001347.
- Zhong, J., W. Wang, X. Yue, A. G. Burns, X. Dou, and J. Lei (2016), Long-duration depletion in the topside ionospheric total electron content during the recovery phase of the March 2015 strong storm, *J. Geophys. Res. Space Physics*, *121*, 4733–4747, doi:10.1002/2016JA022469.
- Zhou, Y.-L., H. Lüher, C. Xiong, and R. F. Pfaff (2016), Ionospheric storm effects and equatorial plasma irregularities during the 17–18 March 2015 event, *J. Geophys. Res. Space Physics*, *121*, 9146–9163, doi:10.1002/2016JA023122.